Superconductivity in two-dimensional $NbSe_2$ field effect transistors

2013 Supercond. Sci. Technol. 26 125020

(http://iopscience.iop.org/0953-2048/26/12/125020)

Supercond. Sci. Technol. **26** (2013) 125020 (10pp) doi:10.1088/0953-2048/26/12/125020

Superconductivity in two-dimensional $NbSe_2$ field effect transistors

Mohammed S El-Bana[1,2], Daniel Wolverson[1], Saverio Russo[3], Geetha Balakrishnan[4], Don Mck Paul[4] and Simon J Bending[1]

[1] Department of Physics, University of Bath, Claverton Down, Bath BA2 7AY, UK
[2] Department of Physics, Faculty of Education, Ain Shams University, Cairo, Egypt
[3] Physics, College of Engineering, Mathematics and Physical Sciences, University of Exeter, Exeter EX4 4QL, UK
[4] Department of Physics, University of Warwick, Coventry CV4 7AL, UK

E-mail: mohammed.el-bana@bath.edu

Received 14 August 2013, in final form 5 October 2013
Published 12 November 2013
Online at stacks.iop.org/SUST/26/125020

Abstract
We describe investigations of superconductivity in few molecular layer $NbSe_2$ field effect transistors. While devices fabricated from $NbSe_2$ flakes less than eight molecular layers thick did not conduct, thicker flakes were superconducting with an onset T_c that was only slightly depressed from the bulk value for 2H-$NbSe_2$ (7.2 K). The resistance typically showed a small, sharp high temperature transition followed by one or more broader transitions which usually ended in a wide tail to zero resistance at low temperatures. We speculate that these multiple resistive transitions are related to disorder in the layer stacking. The behavior of several flakes has been characterized as a function of temperature, applied field and back-gate voltage. We find that the conductance in the normal state and transition temperature depend weakly on the gate voltage, with both conductivity and T_c *decreasing* as the electron concentration is *increased*. The application of a perpendicular magnetic field allows the evolution of different resistive transitions to be tracked and values of the zero temperature upper critical field, $H_{c2}(0)$, and coherence length, $\xi(0)$, to be independently estimated. Our results are analyzed in terms of available theories for these phenomena.

(Some figures may appear in colour only in the online journal)

1. Introduction

The first isolation of graphene in 2004 [1] has led to a resurgence of interest in the study of layered materials. In particular it has been shown that these can form the basis of truly two-dimensional atomic crystals with remarkable electronic properties and very high specific surface areas, making them suited for applications ranging from electronic devices to energy storage [2]. The physical insights obtained from working with graphene, as well as a requirement for other 2D materials with complementary electronic properties, has directed attention towards studies of atomically thin forms of the transition metal dichalcogenides (TMDs). These are very promising candidates for nanoscale applications as they exhibit a rich variety of electronic ground states (e.g., metallic, semiconductor, superconductor and charge density wave (CDW)) [3]. One of the more interesting TMDs is the quasi-two-dimensional superconductor niobium diselenide. This has two common hexagonal crystalline forms with slightly different bulk critical temperatures, 2H-$NbSe_2$ and 4H-$NbSe_2$, where the numerical prefix indicates the number of $NbSe_2$ molecules in the unit cell. The 2H-$NbSe_2$ unit cell of interest here contains two $NbSe_2$ molecular layers in AB stacking. Each molecular unit is formed from a sandwich of two layers of Se atoms with a plane of Nb atoms between them, and the coordination numbers of the Se and Nb atoms are 3 and 6, respectively. The lattice constants of 2H-$NbSe_2$ are $a = b = 3.6$ Å and $c = 12.6$ Å, and the spacing between adjacent Nb sheets is thus 6.3 Å [4]. $NbSe_2$ molecular layers are strongly covalently bonded while there is only a weak van der Waals interaction between adjacent layers [5, 6]. Consequently, it is easy to cleave 2H-$NbSe_2$ sheets along planes parallel to the *a*–*b* face and the terminating surface after exfoliation is usually a Se layer [7]. 2H-$NbSe_2$ is metallic at high temperatures but becomes a type II superconductor below a critical temperature of $T_c \simeq 7.2$ K. This material

is believed to be a conventional s-wave superconductor, albeit a highly anisotropic one, and in high quality samples superconductivity coexists with a charge density wave (CDW) which sets in below $T \sim 32$ K. To date there has been little agreement on the nature of the competition between these two ground states [8].

Frindt [7] published the first investigations of few molecular layer 2H-$NbSe_2$ flakes mechanically exfoliated onto various substrates. He observed a decrease in T_c with decreasing flake thickness, a trend that became particularly pronounced in samples estimated to be less than six molecular layers thick. This author was not able to measure flake thicknesses directly but inferred them from the 300 K resistances assuming an effective bulk resistivity of 160 $\mu\Omega$ cm. Using this thickness calibration the T_c of a single molecular layer was predicted to be 3.8 K (cf, $T_c = 7.2$ K in bulk samples). Multiple steps observed in the resistive superconducting transition were associated with regions of the flakes with different thicknesses.

More recently Novoselov *et al* [9] reported measurements of field effect transistors fabricated from single molecular layers of $NbSe_2$ mechanically exfoliated onto Si/SiO_2 substrates. They observed semi-metallic behavior at 300 K with an electron concentration that was two orders of magnitude smaller than that expected from scaling bulk values, suggesting significant changes in the electronic energy spectrum. The dynamic 'field effect' mobility of their devices was measured to be in the range 0.5–3 $cm^2\ V^{-1}\ s^{-1}$, with an *increase* in conductivity as the electron concentration was increased.

In the most recent study of atomically thin $NbSe_2$ flakes Staley *et al* [5] have realized two-terminal field effect transistors fabricated by mechanical exfoliation onto Si/SiO_2 substrates followed by a lithography-free shadow masking contact process. These authors observed superconductivity in devices which were only single unit cells (two molecular layers) thick with T_c as high as 2.5 K. They measured the dynamic mobility for their samples to be in the range $\sim$10–60 $cm^2\ V^{-1}\ s^{-1}$ and observed a clear modulation of T_c with gate voltage in the thinnest flakes. This was interpreted in terms of a simple model for changes in the electronic density of states, but did not address the fact that T_c *decreases* with increasing electron density.

The motivation for this paper is to extend these studies of the field effect on superconductivity in $NbSe_2$ flakes to lithographically defined four-terminal structures in which the number and quality of molecular layers has been fully characterized. It is now well established that the modulation of the charge carrier density in a superconductor can change its physical properties, in particular the superconducting transition temperature T_c. Several conditions must be satisfied in order to observe a measurable electric field effect on superconductivity. Since the carrier density of most metallic superconducting materials is high, a very thin layer of material is needed in order to be able to achieve significant charge density modulation. In addition, a high quality dielectric is important in order to enhance the electric field and allow high gate voltages to be applied. Finally, a good control of material interfaces is crucial in order that the behavior of the device is not undesirably limited by charge redistribution at the flake/substrate and flake/dielectric interfaces rather than changes in the chemical potential of the superconducting flake itself [5]. In our experiments most of these criteria are well satisfied, allowing us to make systematic studies of the electrical properties of thin $NbSe_2$ flakes as a function of temperature, perpendicular magnetic field and back-gate voltage.

2. Experimental method

Our four-terminal field effect devices were fabricated using micromechanical cleavage of high quality 2H-$NbSe_2$ single crystals onto Si/SiO_2 substrates. Optimization of this process using pairs of permanent magnets to apply a controlled pressure allowed flakes up to $\sim$70 μm in size to be exfoliated (cf, figure 1(a)). Substrates were etched in piranha solution prior to exfoliation in order to remove any organic residues from the surface. Highly doped Si substrates with a 297 nm SiO_2 top layer were used as this was found to give good optical contrast for deposited $NbSe_2$ flakes under the microscope. The SiO_2 layer also acts as a robust dielectric allowing the Si substrate to be used as a 'back-gate' up to relatively high voltages ($\sim\pm$100 V). Atomic force microscopy and Raman spectroscopy were used to characterize the quality and number of molecular layers present in our flakes.

Two levels of electron-beam lithography (EBL) were used to define both the inner electrodes (Cr/Au 10/50 nm) and outer bond pads (Cr/Au 20/250 nm) in PMMA, followed by electron-beam deposition of Cr/Au films and lift-off in acetone. In both EBL steps patterns were aligned to markers defined on the Si/SiO_2 wafer by optical lithography prior to exfoliation. The lateral width of electrodes varied from 1–1.5 μm with the spacing between electrodes ranging from 1 to 3 μm (cf, figures 1(b) and (c)). A schematic diagram of a completed $NbSe_2$ field effect transistor is shown in figure 1(d).

Completed devices were wire-bonded in a DIL ceramic package and mounted on a temperature-controlled sample holder which was coupled to a liquid helium bath via exchange gas. Small signal magneto-transport measurements were performed in a variable temperature helium cryostat with a base temperature of 2.0 K. Great care was taken to avoid damage to devices arising from electrostatic shock, and all leads down to the sample were protected with custom-designed pi filters. Four-point measurements were performed with a constant 1 μA 32 Hz ac current, and voltages were detected using a digital lock-in amplifier. Magnetic fields up to 1 T could be applied perpendicular to the $NbSe_2$ flakes with a small superconducting solenoid in the liquid helium bath.

3. Results

3.1. Flake characterization

Several complementary techniques were used to characterize the flakes in our $NbSe_2$ FETs. Single and few-layer

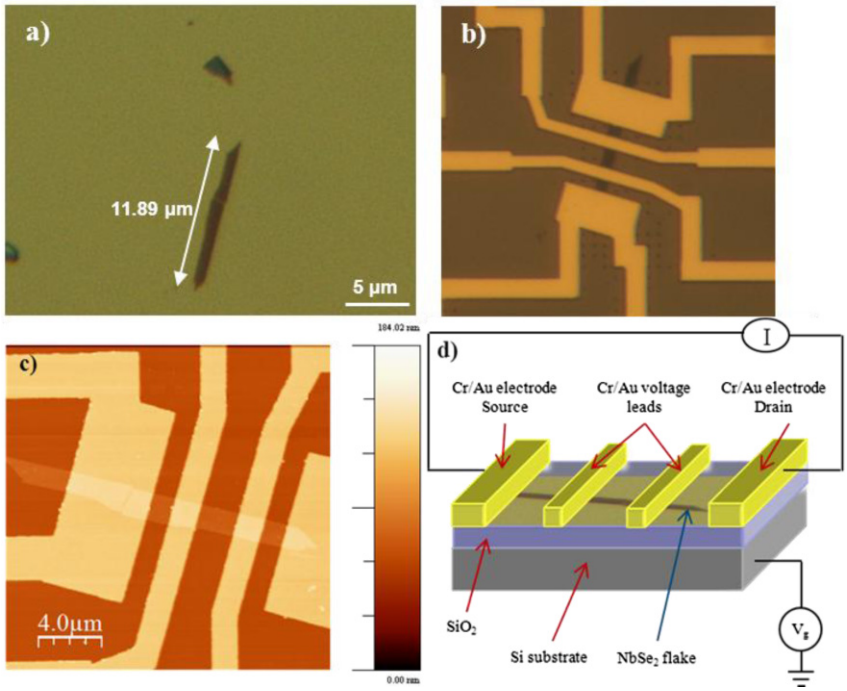

Figure 1. Optical micrographs of the exfoliated flake (a) and the completed device (b). (c) Topographic AFM image for the 7.92 nm thick flake device. (d) Schematic representation of a $NbSe_2$ FET.

Table 1. Flake dimensions, sheet resistance, R_{squ}, bulk resistivity, ρ_{Bulk}, and reduced resistance ratio, RRR, for the four devices studied in detail.

Device thickness, d (nm)	Flake width, W (μm)	Flake length, L (μm)	R_{squ} (Ω) at 300 K	ρ_{Bulk} (Ω cm) at 300 K $\times 10^{-4}$	RRR
6.56 ± 0.38	5.47 ± 0.48	1.66 ± 0.13	1400 ± 0.36	9.20 ± 0.14	—
7.92 ± 0.32	1.56 ± 0.08	2.17 ± 0.22	690 ± 0.18	5.44 ± 0.06	5.27 ± 0.18
9.21 ± 0.35	2.89 ± 0.24	1.34 ± 0.13	1330 ± 0.15	12.2 ± 0.05	5.08 ± 0.12
10.37 ± 0.34	0.70 ± 0.06	1.73 ± 0.19	1170 ± 0.02	12.1 ± 0.1	4.62 ± 0.19

flakes were readily recognized under an optical microscope; different thickness flakes have distinct interference colors with white light illumination. Many of these flakes clearly had regions containing different numbers of molecular layers and only homogeneous ones were selected for device fabrication. Tapping mode atomic force microscopy (AFM) was used to quantitatively measure the thicknesses of $NbSe_2$ flakes (and contacts) on Si/SiO_2 substrates after low temperature electrical measurements had been completed. Although, as is well known for graphene, such AFM estimates could contain systematic errors, samples will henceforth be referred to by these nominal AFM thicknesses which are listed in table 1. AFM was also used to determine the lateral flake dimensions given in this table.

Raman spectroscopy was used to characterize further all of the samples studied. $NbSe_2$ flakes were studied at room temperature under a Renishaw inVia Raman Microscope operating at a 532 nm excitation wavelength. A short working distance 50× objective lens was used to capture Raman spectra from samples with integration times in the range 100–400 s. Figure 2 shows Raman spectra for a selection of flakes of different thicknesses that have all been captured with a laser power of 0.05 mW and an integration time of 100 s. In the thickest samples the out-of-plane phonon mode A_{1g} (228 cm^{-1}) and the in-plane phonon mode E_{2g} (237 cm^{-1}) were well resolved in the Raman spectra. However, decreasing flake thickness tended to be accompanied by a broadening of the two phonon peaks, resulting in almost complete overlap in the thinnest flakes as seen in figure 2. We observe an apparently non-monotonic shift of both phonon modes as the flake thickness is reduced, in agreement with the results of Staley *et al* [5] and Wu *et al* [10]. Hence this shift cannot easily be used to characterize the layer number in $NbSe_2$ in contrast to the situation in few-layer graphene [5] and we propose an explanation for this shift as follows.

Spectra obtained with high laser intensity or long laser exposures were found to evolve with time, and AFM scans revealed that flakes actually thickened after laser exposure. This suggests that structural changes have occurred, of which the most likely are decomposition to produce Se precipitates, or oxidation; in addition, it is known that photo-oxidation of $NbSe_2$ leads to an increase in volume [11]. To resolve this question, we show in figure 3 a series of Raman spectra for a 6.56 nm flake as a function of laser power. These clearly show the appearance of a new peak near 302 cm^{-1} at high

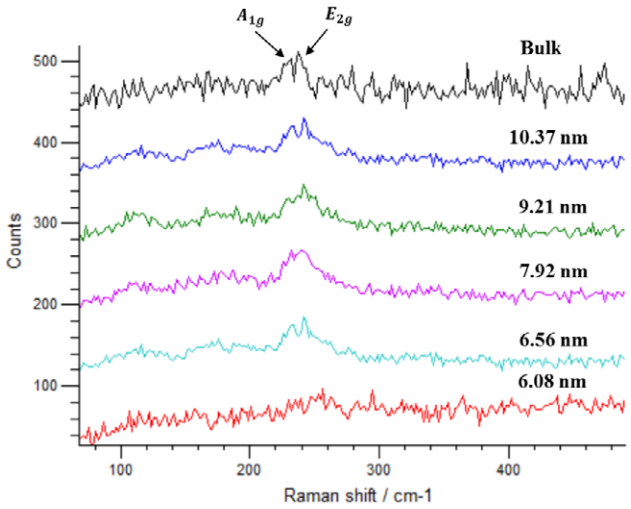

Figure 2. Raman spectra as a function of flake thickness captured with a laser power of 0.05 mW and an integration time of 100 s.

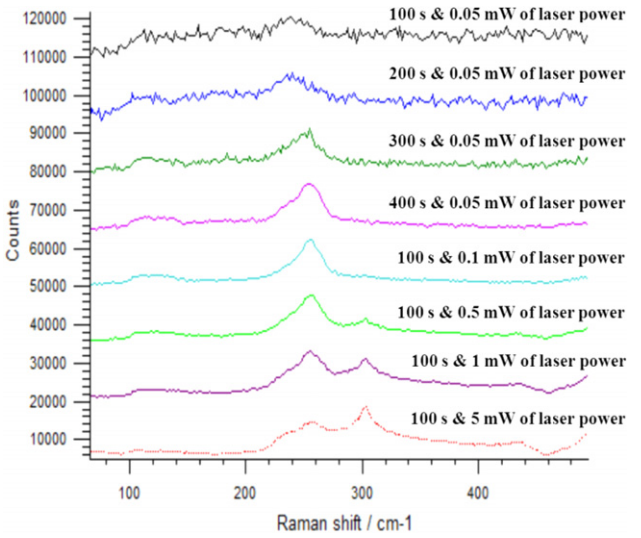

Figure 3. Series of Raman spectra for the same 6.56 nm thick $NbSe_2$ flake as a function of integration time and laser power illustrating the evolution of a new peak near 302 cm^{-1}.

powers (and long times) that is not present in any of our as-fabricated devices under weak illumination; we note that this peak is also evident in figure 2 of Staley *et al* [5], who also comment that laser-induced damage was found for thin flakes. By reference to earlier studies of Raman scattering in niobium oxides [12], we propose that this peak is due to Nb_2O_5 (and not NbO_2). In the bottom spectrum of figure 3, we also observed bands (off scale in the figure) at 620, 670 and 820 cm^{-1}, also consistent with this assignment [12]. Surprisingly, the oxide peaks do not develop in thicker flakes under intense illumination, suggesting that a reduced thermal conductance in thin layers may result in higher temperatures and much more rapid photo-oxidation. Another strong Raman band of Nb_2O_5 is expected to be seen at 996 cm^{-1} but is masked in our case by the second-order Si Raman band; on other substrates, this mode could be a useful diagnostic indicator of oxidation. In summary, our observations suggest that the physical damage due to laser exposure is probably due to photo-oxidation and is more pronounced in very thin flakes. Since Nb_2O_5 also shows strong Raman bands at 240 and 264 cm^{-1} [12] which overlap the E_{2g} mode of $NbSe_2$, it is not surprising that the E_{2g} mode will appear to move non-monotonically with layer thickness whenever oxide formation occurs.

3.2. Electrical and magneto-transport measurements

Systematic electrical measurements as a function of temperature, back-gate voltage and applied magnetic field were successfully performed on four $NbSe_2$ FETs with flake thicknesses in the range 6.56–10.37 nm. Room temperature sheet resistances, R_{squ}, reduced resistance ratios, RRR, and bulk resistivities, ρ_{Bulk}, for the four devices are summarized in table 1. Figure 4 plots the 300 K sheet resistances as a function of inverse thickness. We see that results for three of the devices are quite consistent, but the fourth falls well out of line with these. The dashed trend line on this graph represents a much higher bulk resistivity by a factor of

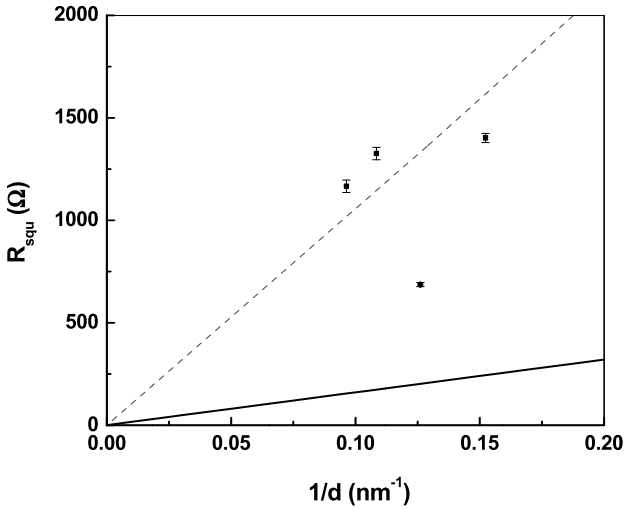

Figure 4. Sheet resistance as a function of inverse flake thickness for several devices. The solid black line represents values estimated from the bulk resistivity of large single crystals ($\rho_{bulk} = 160\ \mu\Omega$ cm) [7].

nearly seven than was assumed in earlier work on $NbSe_2$ by Frindt [7] (lower solid line). Very thin $NbSe_2$ flakes (1–2 unit cell flakes) appeared to be insulating, even though the end-to-end electrode resistances were less than 100 Ω. We speculate that the same reaction processes that occur under intense laser light may happen naturally during device processing, hence each device may have one or more 'dead' molecular layer and the thickness may not be a good measure of the number of electrically conductive layers. In contrast, four-point measurements at temperatures down to ∼2 K on thicker flakes exhibited true zero resistance, as can be seen in figure 5 for a 9.21 nm device. The inset of this figure shows an expanded view of the low temperature resistance data along with its digital derivative, dR/dT, whose smooth dependence indicates the absence of the charge density wave

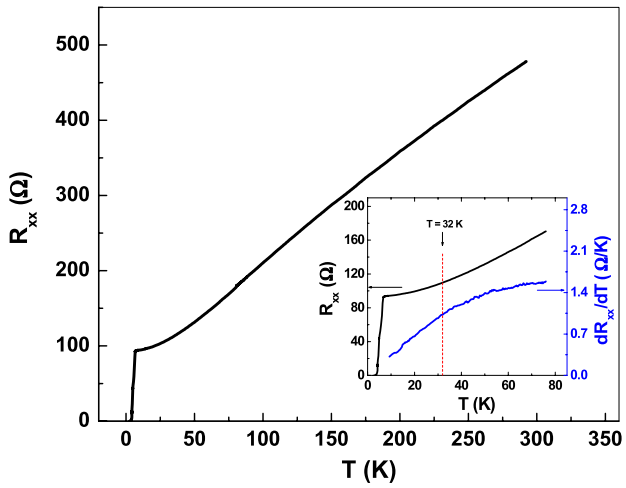

Figure 5. R_{xx} as a function of temperature for the 9.21 nm thick sample. The inset shows an expanded view of the low temperature data and its first derivative confirming the absence of a resistive signature of the CDW transition in this sample.

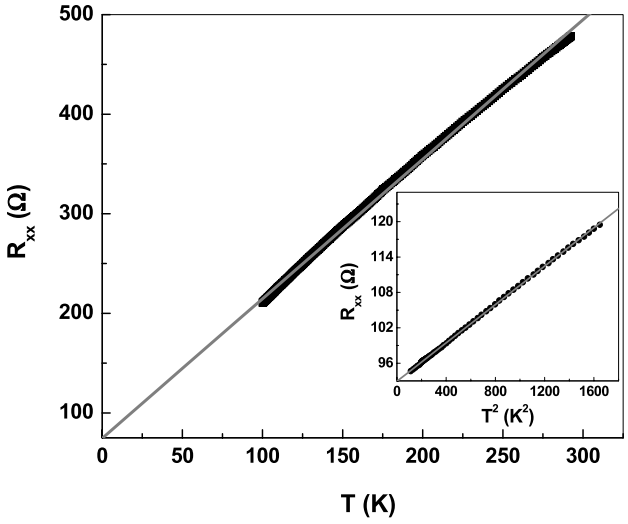

Figure 6. Linear fit obtained assuming $R_{xx} \sim T$ in the 100–300 K temperature range. Inset shows the fit to $R_{xx} \sim T^2$ in the 10–40 K temperature range.

(CDW) transition observed in very high quality samples near $T = 32$ K [13–15]. This was expected for our relatively low mobility $NbSe_2$ samples since it is known that an RRR ~ 30 or higher is needed to observe a CDW [16].

A careful analysis of the temperature-dependent resistance $R_{xx}(T)$ of the 9.21 nm thick device was performed by making power law fits ($\sim T^n$) in the temperature ranges 10–40 and 100–300 K as illustrated in figure 6. A good linear fit has been obtained in the 100–300 K range with $R_{xx} \sim T$, which is in agreement with predictions for a normal metal at temperatures above the Debye temperature Θ (calculated theoretically for $NbSe_2$ to be $\Theta \approx 190$ K [17]). In the range 10–40 K the dependence changed to $R_{xx} \sim T^2$, which can be attributed to electron–electron scattering according to Matthiessen's rule [18].

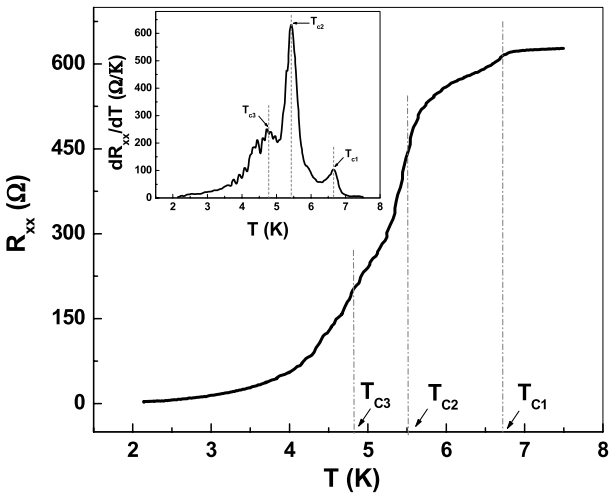

Figure 7. R_{xx} plotted as a function of temperature revealing three distinct superconducting transitions in a 10.37 nm thick device. Inset shows dR/dT which has been used to determine the T_c values.

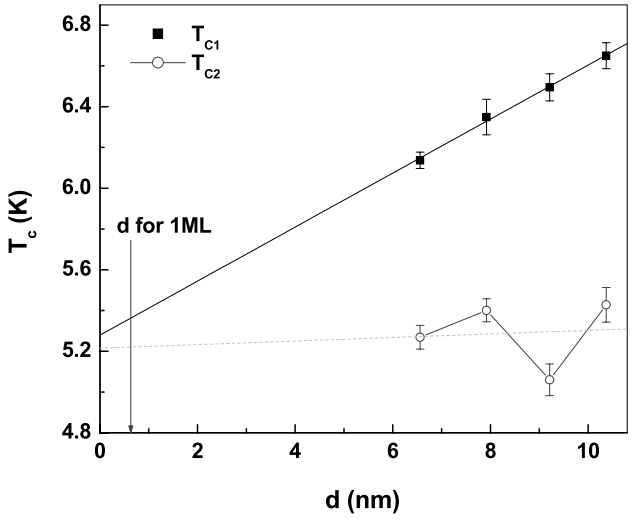

Figure 8. Measured values of resistive transitions T_{c1} and T_{c2} as a function of flake thickness.

Figure 7 shows an expanded view of a typical superconducting resistive transition which reveals signatures of multiple critical temperatures. Indeed all conducting flakes appeared to show at least two resistive transitions, some three. Note that AFM scans indicate that the flakes have a uniform thickness throughout the current-carrying region. Thus, we believe that these multiple resistive transitions are related to disorder in the layer stacking rather than lateral inhomogeneity as was proposed by Frindt [7] as an explanation for similar multiple transitions in his samples. Table 2 shows estimates of the multiple critical temperatures for all samples.

The highest temperature transition T_{c1}, reduces monotonically as the flake thickness is reduced, but the low temperature transitions do not appear to vary particularly systematically. This can be clearly seen in figure 8, where both T_{c1} and T_{c2} are plotted as a function of flake thicknesses. It is interesting that all T_cs seem to extrapolate to approximately

Table 2. A summary of the resistive transitions T_{c1}, T_{c2} and T_{c3}, and the mean field pairing temperature, T_{c0}, estimated from fits to the fluctuation conductivity above T_{c1}.

FET flake thickness (nm)	T_{c1} (K)	T_{c2} (K)	T_{c3} (K)	T_{c0} (K)
6.56 ± 0.38	6.14 ± 0.04	5.27 ± 0.06	—	6.40 ± 0.01
7.92 ± 0.32	6.35 ± 0.09	5.40 ± 0.06	4.99 ± 0.03	6.47 ± 0.01
9.21 ± 0.35	6.50 ± 0.07	5.06 ± 0.08	—	6.55 ± 0.02
10.37 ± 0.34	6.65 ± 0.06	5.43 ± 0.09	4.79 ± 0.12	6.67 ± 0.01

the same value at a thickness corresponding to one molecular layer of $NbSe_2$ ($d = 1$ ML). It is hence possible that the lowest T_cs are associated with single uncoupled $NbSe_2$ molecular layers. This interpretation is in apparent conflict with the much lower estimates of the T_c for 1 ML flakes by Frindt [7] and Staley *et al* [5]. However, it is not unreasonable that this discrepancy arises from very different disorder levels in the various experimental systems used.

A linear suppression of T_c with decreasing thickness can be associated with enhanced Coulomb interactions and a reduction in electron screening arising from increasing disorder and interaction effects. Indeed a complete suppression of superconductivity and formation of an insulating state has been observed in highly disordered flakes [5, 7].

3.2.1. Analysis of the $H = 0$ resistive transition. A more detailed analysis of the $H = 0$ resistive transition has been made for all samples to extract both the mean field pairing temperature, T_{c0}, from the fluctuation conductivity and, when possible, the Berezinskii–Kosterlitz–Thouless vortex–antivortex unbinding temperature, T_{BKT}. The onset T_{c0} values have been estimated by fitting the resistance data above T_{c1} to the Aslamazov–Larkin expression for the fluctuation-enhanced conductivity in 2D samples, $\Delta\sigma(T) \propto \ln(T/T_{c0})^{-1}$ (cf, figure 9(a)) [19]. The estimated T_{c0} values for all samples are listed in table 2. Below T_{c0} it is well established that a loss of global phase coherence and dissipation due to a finite flux resistance occur as a result of the penetration of thermally excited vortices. However, a finite supercurrent can flow below the BKT transition temperature, T_{BKT}, as a consequence of the formation of bound vortex–antivortex pairs due to the attractive interaction between oppositely oriented vortices. The universal form of the flux flow resistance, $R_{xx}(T) \propto \exp[b(T - T_{BKT})^{-1/2}]$, has been used to identify T_{BKT} in our samples. In this expression the constant b is a measure of the strength of the vortex–antivortex interaction [20, 21]. In practice the unbinding temperatures have been extracted by plotting $[1/R_{xx}\mathrm{d}R_{xx}/\mathrm{d}T]^{-2/3}$ versus T at low temperatures and associating the T-axis intercept with T_{BKT} (cf, figure 9). While estimation of T_{BKT} in the 9.21 and 10.37 nm thick samples was straightforward, it could not be achieved reliably in the 6.56 and 7.92 nm thick samples due to the presence of a small zero temperature resistance arising from weak device non-ideality. It is noteworthy that one of these latter two samples shows quite a long low temperature BKT 'tail' while the other does not. It suggests that otherwise similar samples can have very different properties due to different degrees of stacking order [4]. In this case one of the samples appears to behave much more two-dimensionally than the other.

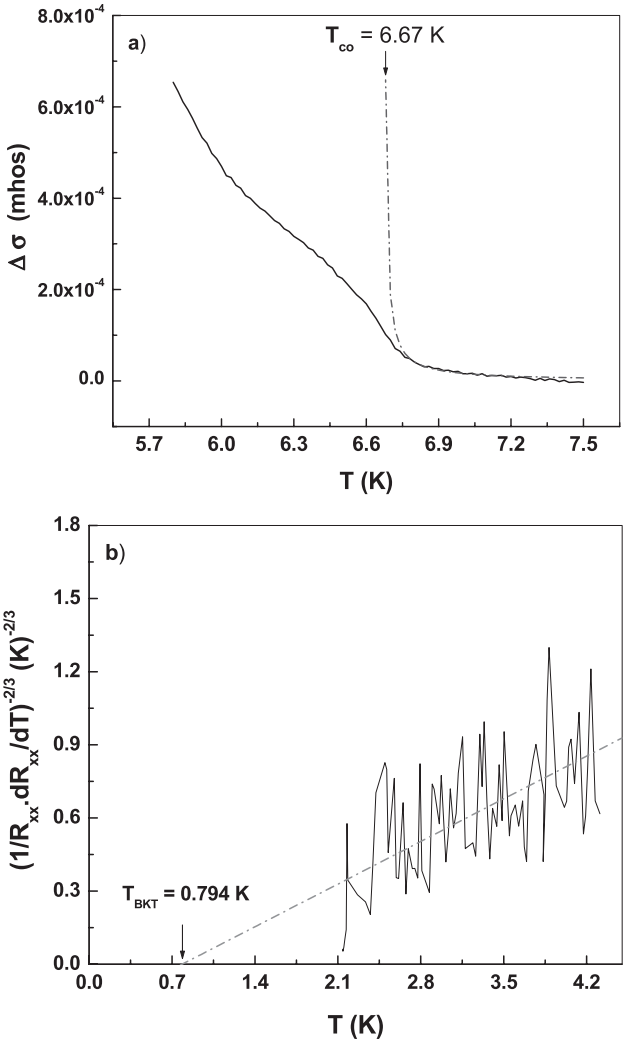

Figure 9. The mean field pairing temperature, T_{c0}, and the vortex–antivortex unbinding transition temperature, T_{BKT}, have been extracted using the Aslamazov–Larkin formula and the universal form of the flux flow resistance respectively for the 10.37 nm thick sample.

3.2.2. Resistive transition behavior as a function of applied magnetic field B. The temperature dependence of the resistance of the 9.21 nm thick sample at various values of magnetic field, B, and of the 10.37 nm device as a function of magnetic field at various values of temperature, T, are shown in figure 10. These data show how the resistive transitions tend to broaden and shift downwards in temperature with increasing magnetic field.

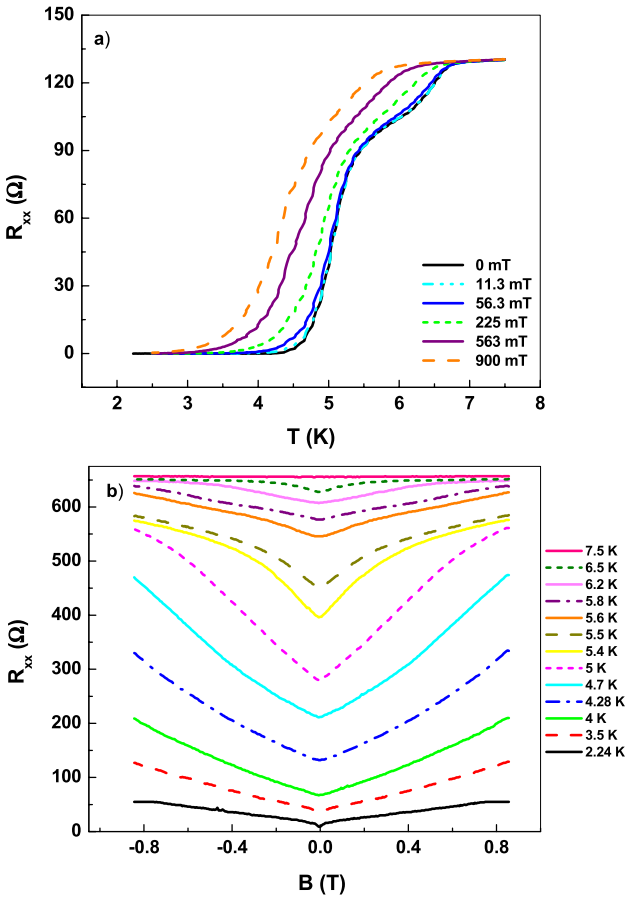

Figure 10. (a) Magnetic field dependence of $R(T)$ for a 9.21 nm thick sample. (b) Temperature dependence of $R(B)$ for a 10.37 nm thick sample.

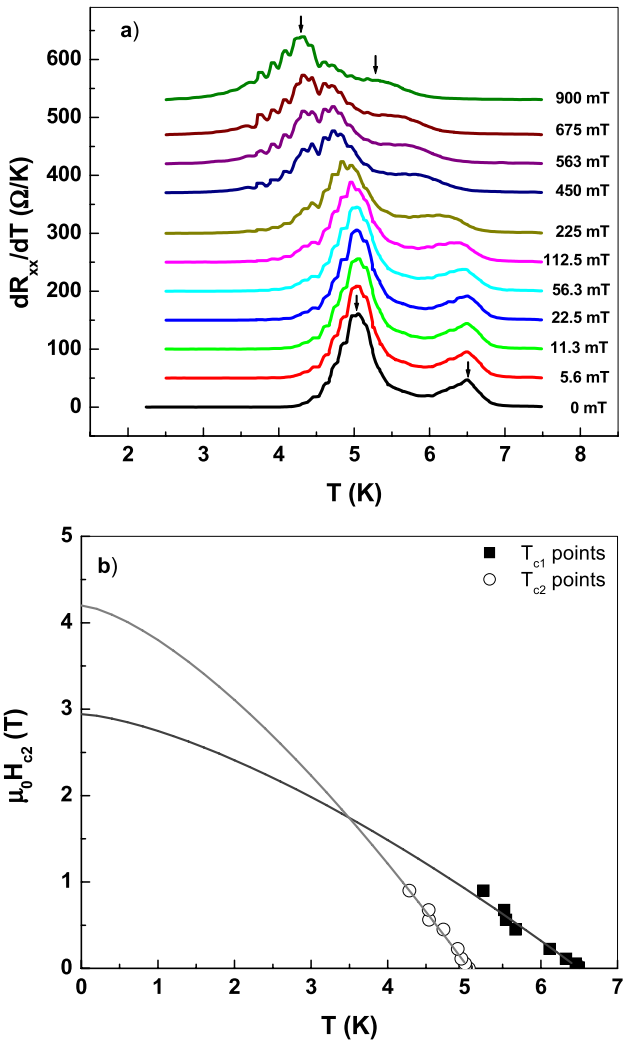

Figure 11. (a) Digital derivative of the $R(T, B)$ for a 9.21 nm thick sample showing the evolution of resistive transitions T_{c1} and T_{c2}. (b) Fits of equation (2) to $T_{c1}(H)$ and $T_{c2}(H)$ as estimated from (a).

We assume that the upper critical field of high critical temperature superconducting 'pockets' controls the observed onset transition shift, whereas the shift in the tails near $R \sim 0$ can be attributed to vortex flow and the field dependence of the vortex–antivortex unbinding transition [22]. The field-dependent resistive transition temperatures have been estimated by determining the position of maximum slope from the first derivative of $R(T)$. The evolution of T_{c1} and T_{c2} as a function of applied magnetic field is plotted in figure 11(a) for the 9.21 nm thick sample. Plots of this type for each sample allow us to calculate the zero temperature upper critical field $H_{c2}(0)$ using the Werthamer–Helfand–Hohenberg (WHH) formula [23]:

$$H_{c2}(0) = -0.69 T_c (dH_{c2}/dT)_{T=T_c}, \quad (1)$$

where T_c is the resistive transition temperature and dH_{c2}/dT is the slope of $H_{c2}(T)$ at T_c.

A different estimation for $H_{c2}(0)$ can be made by using a phenomenological formula based on the Ginzburg–Landau equations for multiband superconductors [24]:

$$H_{c2}(T) = H_{c2}(0)[1 - (T/T_c)^a]^b. \quad (2)$$

When $a = 1/0.69$ and $b = 1$ equations (1) and (2) become mutually consistent, and a good match between estimated values of $H_{c2}(0)$ can be obtained. Taking into account the fact that $NbSe_2$ is a multiband superconductor and $H_{c2}(T)$ is expected to be influenced by this, it is not clear *a priori* which of the two approaches is more appropriate. Figure 11(b) shows fits made using equation (2) for both $T_{c1}(H)$ and $T_{c2}(H)$ for the 9.21 nm thick sample. Knowledge of $H_{c2}(0)$ allows the zero temperature Ginzburg–Landau coherence length, $\xi(0)$, to be calculated from the well-known relationship [25]

$$H_{c2}(0) = \phi_0/2\pi\xi(0)^2, \quad (3)$$

where ϕ_0 is the superconducting flux quantum. Values calculated for $H_{c2}(0)$ and $\xi(0)$ are summarized in table 3, and are in reasonably good agreement with other literature values [24, 26].

3.2.3. The influence of a back-gate voltage. Figure 12 shows the longitudinal conductivity, σ_{xx}, of the 10.37 nm thick sample as a function of V_g at $T = 7$ K. The data show an approximately linear *reduction* in conductivity with gate voltage, and the slope, $\Delta\sigma_{2D}/\Delta V_g$, allows one to calculate

Table 3. Table of the zero temperature upper critical field, $H_{c2}(0)$, and GL coherence length, $\xi(0)$, as estimated for three of the devices using equation (2).

	$H_{c2}(0)$ (T)		$\xi(0)$ (Å)	
FET flake thickness (nm)	T_{c1}	T_{c2}	T_{c1}	T_{c2}
7.92 ± 0.32	3.30 ± 0.19	2.67 ± 0.18	98.2 ± 0.1	109.0 ± 0.1
9.21 ± 0.35	2.94 ± 0.14	4.2 ± 0.22	104.0 ± 0.1	87.1 ± 0.1
10.37 ± 0.34	3.93 ± 0.23	3.94 ± 0.26	90.0 ± 0.1	89.9 ± 0.1

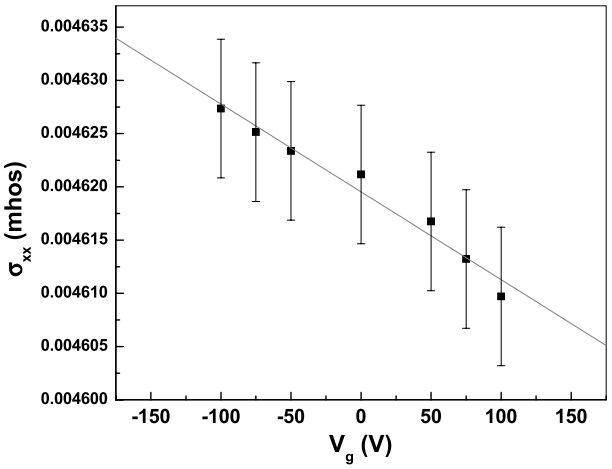

Figure 12. Plot of the longitudinal conductivity as a function of applied gate voltage, V_g, for a 10.37 nm thick sample at $T = 7$ K.

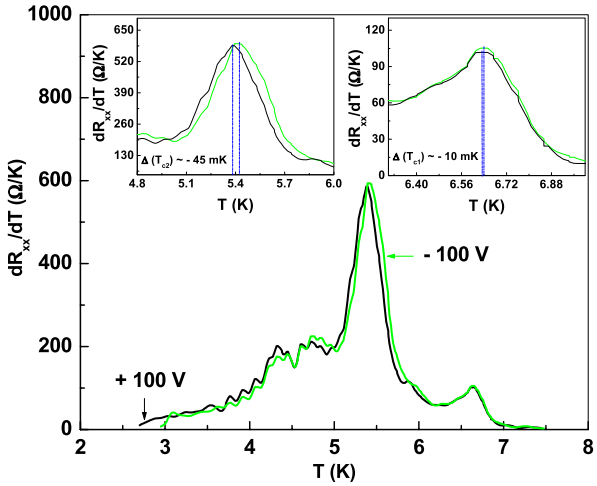

Figure 13. Plots of dR_{xx}/dT versus temperature showing the influence of a back-gate voltage on the resistive superconducting transition of the 10.37 nm thick sample. Insets show expanded views of the changes around T_{c1} and T_{c2}.

the dynamic field effect mobility, μ_{FE}, from [27]:

$$\mu_{FE} = \frac{d}{\varepsilon_r \epsilon_0} \frac{\Delta\sigma_{2D}}{\Delta V_g}, \tag{4}$$

where d is the SiO_2 layer thickness, ε_r is the relative dielectric constant of SiO_2 ($\varepsilon_r = 3.9$) and ϵ_0 is the permittivity of free space. This rather indirect way to estimate the mobility of our devices is valuable since they have not been fabricated in a Hall bar configuration. The calculated dynamic mobilities μ_{FE} for our devices lie in the range of 7–64 $cm^2\ V^{-1}\ s^{-1}$ at 7 K, which is in agreement with the findings of Staley *et al* [5] but many orders of magnitude higher than values reported by Novoselov *et al* [9]. Moreover, the observation that the conductivity *decreases* at positive gate voltages is in conflict with these latter results.

Finally we have investigated the influence of applied gate voltages of −100 and +100 V on the resistive transition of samples. We observe a weak *reduction* in the resistive transition temperatures with more positive gate voltages. Figure 13 shows the digital derivative, dR/dT, of the temperature-dependent sheet resistance of a 10.37 nm thick sample at $V_g = -100$ and +100 V in order to enhance the small shifts observed with gate voltage. The shift in T_c between these two values of V_g was estimated to be −10 mK and −45 mK for T_{c1} and T_{c2}, respectively.

4. Discussion

Patterning four-terminal transport structures allows almost ideal measurements in which the influence of contact resistances is eliminated. This distinguishes our results from the two-terminal measurements of Staley *et al* [5], while Frindt [7] does not actually state how measurements were made. Moreover, we are able to directly measure the thickness of our flakes and hence calculate an accurate value for the effective 300 K bulk resistivity that is seven times larger than typical values in single crystals, suggesting that Frindt's flake thicknesses may possibly have been considerably underestimated. One potential drawback of the use of lithographic patterning is that it may lead to the introduction of strain and stacking disorder. Staley *et al* [5] did not report multiple resistive transitions in their shadow masked devices, although the superconducting transitions they show in their paper do appear to be relatively broad.

The three most common polytypes of niobium diselenide are 2H-$NbSe_2$, 4H-$NbSe_2$ and 3R-$NbSe_2$. The first two hexagonal structures exhibit superconductivity below 7.2 K and 6.3 K, respectively. In contrast, the third rhombohedral structure is not superconducting down to 1.2 K [28]. This illustrates rather graphically that the critical temperature of $NbSe_2$ depends very strongly on quite subtle changes in layer stacking. BCS theory tells us that this dependence can arise from both the density of electronic states near the Fermi energy and the phonon spectrum via the electron–phonon coupling strength. It is well established that the former depends quite strongly on the number of molecular layers [29, 30] as well as their stacking. Likewise the phonon

spectrum is also known to depend on the number of layers [30], in particular the low frequency breathing and shear modes [31]. The observed multiple resistive transitions must arise from lateral material inhomogeneities; if there were only vertical inhomogeneities down through the ML stack the low T_c regions would be shorted by the highest T_c region and only one high temperature transition would be observed. We infer from the relatively large amplitude of low temperature resistive transitions that they arise from quite large regions with different stacking order or strain, induced during mechanical exfoliation or lithographic processing. Only the small amplitude, high temperature, resistive transition shifts systematically downwards in thinner flakes, consistent with the expected dependence of the density of electronic states and phonon spectrum on the number of ML combined with enhanced Coulomb interactions and a reduction in electron screening arising from increasing disorder and interaction effects. The systematic linear dependence of T_{c1} on thickness suggests that it is a local property of all coupled molecular layers in the flake, possibly arising from small, well-separated pockets of superconductivity in a normal matrix. Such non-uniformities could be the consequence of disorder due to extrinsic charges in the adjacent SiO_2 dielectric or adsorbed molecules on the surface of the flake (cf, the formation of electron/hole puddles in graphene [32]).

The lowest temperature transitions seem to be truly two-dimensional in nature with resistive tails dominated by the BKT vortex–antivortex unbinding transition. Normally the suppression of T_{BKT} well below the mean field transition temperature, as is the case in most of our samples, is only observed in highly disordered thin films with very short mean free paths. Simple estimates of the sheet resistance for a single $NbSe_2$ ML indicate that we are not in this limit. However, it is known that the attractive vortex–antivortex interaction in 2D superconductors can be substantially screened through a material-dependent dielectric constant, ϵ_v, that linearly scales down T_{BKT} ($T_{BKT} \propto 1/\epsilon_v$) [33]. Hence the low value of T_{BKT} observed in most of our flakes suggests a relatively large screening parameter, ϵ_v, leading to weakly bound vortices and antivortices.

Fits of WHH theory to $H_{c2}(T)$ for the different resistive transitions reveal quite a large scatter in $H_{c2}(0)$ and $\xi(0)$ with no systematic variation as a function of flake thickness. The measured $T = 0$ critical fields of ~3–4 T are considerably lower than typical values for bulk single crystals ($H_{c2}(0) \sim$ 14.6 T [26]), partly due to the reduced critical temperatures for our flakes. Surprisingly the estimated coherence lengths of ~9–11 nm are slightly larger than those measured in single crystals ($\xi(0) \sim 7.7$ nm [26]). This is not what one would expect since the high levels of disorder in our flakes should lead to a significant reduction in $\xi(0)$.

The decrease of normal state conductance and resistive transition temperatures with increased electron concentration is consistent with recent pseudopotential DFT calculations of the electronic density of states in few molecular layer 2H-$NbSe_2$ [29]. These predict a sharp peak about 100 meV below the Fermi energy and a strong downward slope as it crosses E_F. Since the application of a gate voltage would not be expected to significantly change the phonon spectrum or electron–phonon coupling, a reduction in density of electronic states would also account for the observed reduction in T_c. The fact that the low temperature transitions shift more than four times faster with gate voltage than the small high temperature transition indicates that the former are associated with layers that lie closer to the SiO_2 gate dielectric where electric fields are strongest.

Future work will focus on improving the electronic properties (e.g., mobility, carrier concentration, back-gate efficiency) of 2H-$NbSe_2$ flakes. In particular, it appears that the act of patterning contacts may be enough to create strain in the flakes and induce layer stacking disorder. It would be interesting to compare with devices prepared with a lithography-free technique, e.g., shadow masking as used by Staley *et al* [5], which could yield higher mobilities and lower levels of strain. Exfoliation onto a different substrate such as CVD h-BN should also greatly reduce levels of disorder arising from extrinsic charges in the SiO_2 dielectric. The ability to apply larger electric fields will also lead to much larger shifts in T_c and replacing SiO_2 by a higher permittivity gate dielectric, e.g., HfO_2, could enhance FET performance as demonstrated by Zhang *et al* [34] in ambipolar MoS_2 FETs. Finally, accurate calculations of the electronic band structure (and DOS), phonon spectrum and electron–phonon coupling in $NbSe_2$ flakes with different layer stacking orders are urgently required to inform experimental work. These theoretical studies will need to be complemented by detailed structural characterization of our samples (e.g., by STM/STS or HRTEM) in order to obtain a systematic understanding of the behaviors we have observed.

5. Conclusions

In conclusion, systematic investigations of superconductivity in few molecular layer $NbSe_2$ flakes have been performed in well-characterized four-terminal devices produced by mechanical exfoliation from a 2H-$NbSe_2$ single crystal onto Si/SiO_2 substrates. While devices fabricated from extremely thin $NbSe_2$ flakes did not appear to conduct, slightly thicker flakes were superconducting with an onset T_c that was only slightly depressed from the bulk value. All devices exhibited multiple resistive transitions, even though AFM scans confirmed that flakes were of uniform thickness. We attribute this to local regions of strain and layer stacking disorder in our samples. The application of a positive back-gate voltage (increased electron density) led to a weak reduction in conductivity and critical temperature consistent with recent calculations of the electronic density of states. Measurements of $H_{c2}(T)$ reveal that $H_{c2}(0)$ is strongly suppressed while surprisingly $\xi(0)$ is significantly increased with respect to typical values for bulk 2H-$NeSe_2$. A complete understanding of the observed phenomena will require careful characterization of the stacking order in our samples combined with a detailed theoretical analysis of the band structure, phonon spectrum and electron–phonon coupling of realistic $NbSe_2$ flakes. This work should inform investigations of other 2D superconducting crystals in common layered

materials allowing the exploration of new physics and possible device applications.

Acknowledgments

The authors acknowledge financial support from the Egyptian government and Ain Shams University, EPSRC in the UK under grant no. EP/G036101/1 and the NanoSC COST Action MP-1201. SR acknowledges financial support from EPSRC grant nos. EP/K010050/1, EP/J000396/1 and EP/G036101/1.

References

[1] Novoselov K, Geim A K, Morozov S, Jiang D, Zhang Y, Dubonos S, Grigorieva I and Firsov A 2004 Electric field effect in atomically thin carbon films *Science* **306** 666–9
[2] Coleman J N *et al* 2011 Two-dimensional nanosheets produced by liquid exfoliation of layered materials *Science* **331** 568–71
[3] Benameur M, Radisavljevic B, Heron J, Sahoo S, Berger H and Kis A 2011 Visibility of dichalcogenide nanolayers *Nanotechnology* **22** 125706
[4] Mattheis L F 1973 Band structures of transition-metal-dichalcogenide layer compounds *Phys. Rev.* B **8** 3719–40
[5] Staley N E, Wu J, Eklund P, Liu Y, Li L J and Xu Z 2009 Electric field effect on superconductivity in atomically thin flakes of $NbSe_2$ *Phys. Rev.* B **80** 184505
[6] Wang Q H, Kalantar-Zadeh K, Kis A, Coleman J N and Strano M S 2012 Electronics and optoelectronics of two-dimensional transition metal dichalcogenides *Nature Nanotechnol.* **7** 699–712
[7] Frindt R F 1972 Superconductivity in ultrathin $NbSe_2$ layers *Phys. Rev. Lett.* **28** 299–301
[8] Borisenko S V *et al* 2008 Pseudogap and charge density waves in two dimensions *Phys. Rev. Lett.* **100** 196402
[9] Novoselov K S, Jiang D, Schedin F, Booth T J, Khotkevich V V, Morozov S V and Geim A K 2005 Two-dimensional atomic crystals *Proc. Natl Acad. Sci. USA* **102** 10451–3
[10] Wu Y, An M, Xiong R, Shi J and Zhang Q 2008 Raman scattering spectra in the normal phase of 2H-$NbSe_2$ *J. Phys. D: Appl. Phys.* **41** 175408
[11] Myers G and Montet G 1971 Light-induced oxidation of $NbSe_2$ single crystals *J. Phys. Chem. Solids* **32** 2645–6
[12] Huang B X, Wang K, Church J S and Li Y-S 1999 Characterization of oxides on niobium by Raman and infrared spectroscopy *Electrochim. Acta* **44** 2571–7
[13] Corcoran R, Meeson P, Onuki Y, Probst P-A, Springford M, Takita K, Harima H, Guo G and Gyorffy B 1994 Quantum oscillations in the mixed state of the type II superconductor 2H-$NbSe_2$ *J. Phys.: Condens. Matter* **6** 4479
[14] Stiles J, Williams D L and Zuckermann M 1976 Dependence of the critical temperature for the formation of charge density waves in 2H-$NbSe_2$ upon impurity concentration *J. Phys. C: Solid State Phys.* **9** L489
[15] Berthier C, Molinié P and Jérome D 1976 Evidence for a connection between charge density waves and the pressure enhancement of superconductivity in 2H-$NbSe_2$ *Solid State Commun.* **18** 1393–5
[16] Iwaya K, Hanaguri T, Koizumi A, Takaki K, Maeda A and Kitazawa K 2003 Electronic state of $NbSe_2$ investigated by STM/STS *Physica* B **329** 1598–9
[17] Naito M and Tanaka S 1982 Electrical transport properties in 2H-NbS_2, $NbSe_2$, TaS_2 and $TaSe_2$ *J. Phys. Soc. Japan* **51** 219–27
[18] Volkenshtein N, Dyakina V and Startsev V 1973 Scattering mechanisms of conduction electrons in transition metals at low temperatures *Phys. Status Solidi* b **57** 9–42
[19] Aslamazo L G and Larkin A I 1968 Influence of fluctuation pairing of electrons on conductivity of normal metal *Phys. Lett.* A **A26** 238–9
[20] Minnhagen P 1987 The two-dimensional Coulomb gas, vortex unbinding, and superfluid–superconducting films *Rev. Mod. Phys.* **59** 1001–66
[21] Kessler B M, Girit C O, Zettl A and Bouchiat V 2010 Tunable superconducting phase transition in metal-decorated graphene sheets *Phys. Rev. Lett.* **104** 047001
[22] Zhu X, Yang H, Fang L, Mu G and Wen H-H 2008 Upper critical field, Hall effect and magnetoresistance in the iron-based layered superconductor $LaFeAsO_{0.9}F_{0.1-\delta}$ *Supercond. Sci. Technol.* **21** 105001
[23] Werthamer N, Helfand E and Hohenberg P 1966 Temperature and purity dependence of the superconducting critical field, H_{c2}. III. Electron spin and spin–orbit effects *Phys. Rev.* **147** 295
[24] Zehetmayer M and Weber H 2010 Experimental evidence for a two-band superconducting state of $NbSe_2$ single crystals *Phys. Rev.* B **82** 014524
[25] Tinkham M 2004 *Introduction to Superconductivity* vol 1 (New York: Dover)
[26] Banerjee S, Patil N, Ghosh K, Saha S, Menon G, Ramakrishnan S, Grover A, Mishra P, Rao T and Ravikumar G 1997 Magnetic phase diagram of anisotropic superconductor 2H-$NbSe_2$ *Physica* B **237** 315–7
[27] Staley N E, Puls C P and Liu Y 2008 Suppression of conductance fluctuation in weakly disordered mesoscopic graphene samples near the charge neutral point *Phys. Rev.* B **77** 155429
[28] Andreeva O, Braude I and Mamalui A 2012 Selenium vacancies and their effect on the fine structure of $NbSe_2$ quasi-two-dimensional single crystals *Phys. Met. Metallogr.* **113** 888–92
[29] Lebègue S and Eriksson O 2009 Electronic structure of two-dimensional crystals from *ab initio* theory *Phys. Rev.* B **79** 115409
[30] Calandra M, Mazin I and Mauri F 2009 Effect of dimensionality on the charge-density wave in few-layer 2H-$NbSe_2$ *Phys. Rev.* B **80** 241108
[31] Molina-Sánchez A and Wirtz L 2011 Phonons in single-layer and few-layer MoS_2 and WS_2 *Phys. Rev.* B **84** 155413
[32] Allain A, Han Z and Bouchiat V 2012 Electrical control of the superconducting-to-insulating transition in graphene–metal hybrids *Nature Mater.* **11** 590–4
[33] Epstein K, Goldman A and Kadin A 1982 Renormalization effects near the vortex-unbinding transition of two-dimensional superconductors *Phys. Rev.* B **26** 3950
[34] Zhang Y, Ye J, Matsuhashi Y and Iwasa Y 2012 Ambipolar MoS_2 thin flake transistors *Nano Lett.* **12** 1136–40